Planetary and Space Science xxx (2017) 1–6

Contents lists available at ScienceDirect

Planetary and Space Science

journal homepage: www.elsevier.com/locate/pss

Carbon-rich dust from the asymptotic giant branch to planetary nebulae

G.C. Sloan [a, b, c, *]

[a] Department of Physics and Astronomy, University of North Carolina, Chapel Hill, NC 27599-3255, USA
[b] Space Telescope Science Institute, Baltimore, MD 21218, USA
[c] Cornell Center for Astrophysics and Planetary Science, Cornell University, Ithaca, NY 14850-6801, USA

ARTICLE INFO

Keywords:
Carbon stars
AGB stars
Planetary nebulae
Dust

ABSTRACT

As carbon stars evolve from the asymptotic giant branch to planetary nebulae, the spectrum from the dust around them changes from a mixture dominated by amorphous carbon to one dominated by polycyclic aromatic hydrocarbons (PAHs). Along the way, many other components appear, including SiC and MgS, aliphatic hydrocarbons, the still unidentified 21 μm emission feature, and fullerenes. The evidence from infrared spectral surveys suggests that the dust can form with layered structures, that aliphatics can co-exist with the PAHs in post-AGB objects, and that the appearance of the 21 μm feature is associated with aliphatics. Many uncertainties remain. Perhaps the most important is the composition of the amorphous carbon that dominates dust on the AGB, because different compositions can change the total dust output from carbon stars by nearly an order of magnitude.

1. Introduction

I was asked to review the properties of carbon-rich dust from the asymptotic giant branch (AGB) to planetary nebulae (PNe). To complete this task, I have relied heavily on studies of the spectral properties of carbon-rich objects in the Magellanic Clouds and other nearby dwarf galaxies in the Local Group using the Infrared Spectrograph (IRS; Houck et al., 2004) on the *Spitzer Space Telescope* (Werner et al., 2004). The spectra were obtained in a series of observing programs by many different investigators, which as a whole gives us a unique look at how the composition and quantity of dust produced by AGB stars depend on their initial mass and metallicity.

While I am writing as a single author, the conclusions drawn here are based on the work of many collaborators, many of whom have contributed as coauthors of two recent papers. Sloan et al. (2016) considered the complete sample of Magellanic carbon stars observed by IRS, and Sloan et al. (2014) similarly tackled the smaller IRS sample of carbon-rich post-AGB objects and young PNe.

The thorough review of mass loss and dust production by AGB stars by Habing (1996) remains an excellent starting point on the subject, even if it is now two decades old. Here, we will only touch on the key points. Carbon stars result from the dredge-up of carbon produced via the triple-α sequence in the helium-rich layer around the cores of AGB stars. At solar metallicities, stars with initial masses from ~2 to 5 $M_\odot$ become carbon stars, with both the lower and upper limits dropping at lower metallicity, to ~1.4–4 $M_\odot$ in the SMC (Karakas and Lattanzio, 2007). The outflows from these stars will be carbon-rich, because the formation of CO will continue until the less abundant element, O, is consumed, leaving the excess C available to form dust. Stars fusing helium to carbon in their cores are unstable to pulsations in their envelopes, so that they are observed as long-period variables (LPVs). Stars pulsating with the strongest amplitudes are classified as Mira variables. In the Magellanic Clouds, the Miras are associated with the production of carbon-rich dust, while carbon-rich variables with weaker amplitudes (semi-regular and irregular variables) generally show molecular absorption features, but little dust, in their spectra (e.g., Sloan et al., 2015).

2. Dust around carbon stars on the AGB

Sloan et al. (2006) and Zijlstra et al. (2006) published the first IRS-based studies of carbon stars in the Small and Large Magellanic Clouds (SMC and LMC). They introduced the Manchester Method, which relies on a standard set of analysis steps to compare the properties of large samples of IRS spectra. The key metric is the [6.4]−[9.3] color, which samples two wavelength regions relatively free of absorption bands from molecules or emission features from dust and gives a good idea of the relative contributions from the stellar photosphere and from amorphous carbon dust. While most dust species produce readily identifiable emission features in the infrared, amorphous carbon has no infrared resonances, and its presence is best detected using color indices

* Corresponding author. Department of Physics and Astronomy, University of North Carolina, Chapel Hill, NC 27599-3255, USA.
E-mail address: sloan@astro.cornell.edu.

http://dx.doi.org/10.1016/j.pss.2017.07.017
Received 30 November 2016; Received in revised form 23 May 2017; Accepted 25 July 2017
Available online xxxx

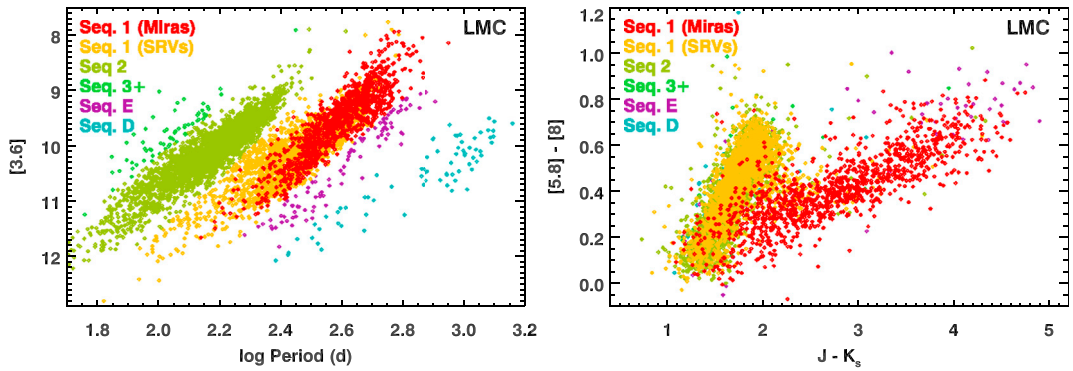

Fig. 1. The relation between stellar pulsation and the production of dust by carbon stars. The left-hand panel plots the apparent magnitude at 3.6 μm vs. Pulsation period. The sources are color-coded by the sequence they are on, with sources on the fundamental mode (sequence 1) subdivided by their pulsation amplitude into Mira variables and semi-regular variables (SRVs). In the right-hand panel, the Miras dominate the sequence of dusty carbon stars characterized by increasingly red $J-K_s$ colors as the [5.8]−[8] color increases, while the lower-amplitude variables and variables on other sequences dominate the sequence of relatively dust-free carbon stars with $J-K_s \lesssim 2$. (For interpretation of the references to colour in this figure legend, the reader is referred to the web version of this article.)

like [6.4]−[9.3]. Sloan et al. (2008), using radiative transfer models published by Groenewegen et al. (2007), showed that the [6.4]−[9.3] color tracks the log of the dust-production rate.

2.1. Dust production and stellar pulsation

Dust production and stellar pulsation are closely related. In the Magellanic Clouds, nearly all of the dust-producing carbon stars are Mira variables, and vice versa. Furthermore, the amount of dust increases with pulsation period and with pulsation amplitude.

Our understanding of LPVs in the Magellanic Clouds has benefited enormously from surveys like the Optical Gravitational Lensing Experiment (OGLE, Udalski et al., 1992) and the Massive Compact Halo Object project (MACHO, Alcock et al., 1992). Fig. 1 illustrates their power. The left-hand figure plots the 3.6 μm magnitude from the *Spitzer* survey of the LMC (Meixner et al., 2006) as a function of the pulsation period measured by the OGLE-III survey of the LMC (Soszyński et al., 2009). The various sequences are labeled following the conventions of Fraser et al. (2005). Stars pulsating in the fundamental mode appear on Sequence 1. Overtone pulsators appear on Sequences 2 and higher. The Miras and SRVs are distinguished by their pulsation amplitudes in the OGLE-III survey, with the Miras having the larger amplitudes.

The right-hand panel in Fig. 1 shows two distinct sequences. The sequence dominated by SRVs and overtone pulastors stays to the blue of $J-K_s \sim 2$, but reddens quickly in [5.8]−[8] due to increasing molecular absorption in the 5.8 μm filter, while the sequence dominated by Miras shows significant reddening in $J-K_s$ from optically thick dust in the circumstellar shell. These results mirror those for the SMC published by Sloan et al. (2015).[1]

Fig. 2 plots the [6.4]−[9.3] color, which measures the dust-production rate, versus the pulsation period of the Miras. In general, the longer the pulsation period, the more dust the star produces.

Fig. 3 (left) shows that the dust-production rate also depends on pulsation amplitude. This figure plots the standard deviation of several epochs at 3.6 μm versus [5.8]−[8] color and codes the data by their [6.4]−[9.3] color. Sloan et al. (2016) showed that the two colors are closely related. Out to [5.8]−[8] ∼ 1.5, increasing pulsation amplitude leads to redder colors, indicating more circumstellar dust.

2.2. Dust production and metallicity

Fig. 2 includes carbon stars from the Galaxy, LMC, SMC, and three nearby dwarf spheroidals. The galaxies show similar relationships between dust content and pulsation period despite their differences in metallicity, but the scatter in the relationship is considerable. The most metal-poor dwarf spheroidal galaxies considered, Sculptor and Leo I, do show a slight drop in the dust-period relation, but they are still within the overall envelope of the data. Sloan et al. (2016) found that the scatter in the Magellanic samples results from the range of initial masses of the stars, with more massive stars pulsating with a longer period for a given amount of dust. They compared the relation between dust content and pulsation period for the LMC and SMC samples, taking into account differences in their initial mass distributions, but were still unable to find a statistically significant difference in the relation from the two galaxies.

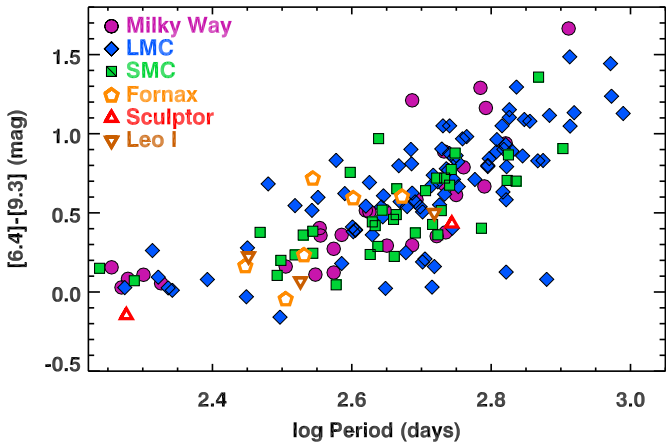

Fig. 2. The carbon-rich dust content, as measured by the [6.4]−[9.3] color, as a function of pulsation period. Stars pulsating with longer periods are associated with more circumstellar dust, with significant scatter and no distinction between the populations from the galaxies, despite their differences in metallicity (data from Sloan et al., 2012, 2016). (For interpretation of the references to colour in this figure legend, the reader is referred to the web version of this article.)

While we do not see much difference in dust production with metallicity star for star, the number of carbon stars increases at lower metallicity, because the lower mass limit for carbon stars has decreased. The result is a higher fraction of carbon stars and a higher fraction of carbon-rich dust ejected by evolved stars (e.g. Blanco et al., 1978, 1980; Cioni and Habing, 2003; Matsuura et al., 2009, 2013; Boyer et al., 2012).

2.3. Extremely red objects and evolution off the AGB

The reddest, most embedded sources in Fig. 3 have been described as extremely red objects (EROs; Gruendl et al., 2008). Most dusty carbon stars show a broad emission feature centered at ∼11.3 μm from SiC dust, but in the EROs, this feature is in *absorption*. These objects are less

[1] Sloan et al. (2015) had inadvertently reversed Sequences D and E, an error which is corrected here.

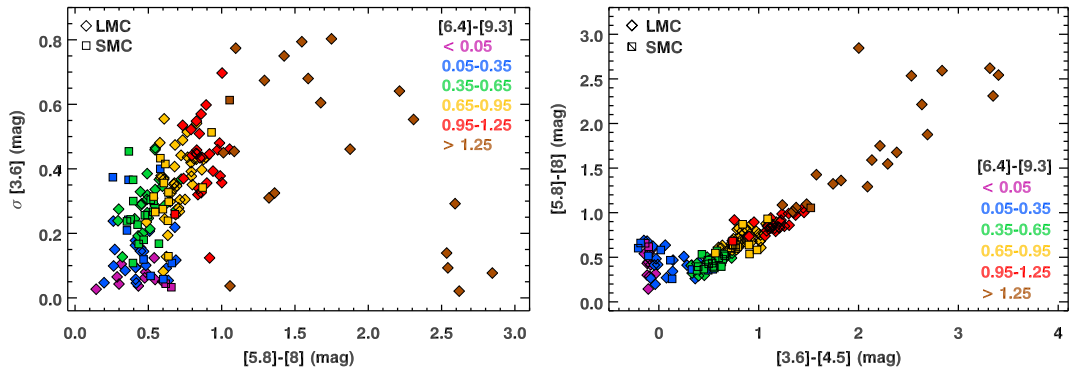

Fig. 3. Left: Pulsation amplitude, as measured by the standard deviation at 3.6 μm, versus [5.8]−[8] color. For most of the sample, the amplitude and dust content rise together, but the reddest sources show surprisingly low pulsation amplitudes. Right: The infrared colors show that the reddest sources (in [5.8]−[8]) have left the sequence of carbon stars, likely because emission from the central star is getting through a dissipating or asymmetric dust shell at shorter wavelengths. (For interpretation of the references to colour in this figure legend, the reader is referred to the web version of this article.)

variable compared to less dusty objects, suggesting that they may actually be evolving off of the AGB. The right-hand panel of Fig. 3 shows that these objects can be unexpectedly blue at shorter wavelengths, as though the central star is peeking through the circumstellar dust shell, perhaps because it is growing patchy or the dust is distributed asymmetrically (Sloan et al., 2016).

2.4. Layering in carbonaceous grains

Forrest et al. (1981) discovered the feature peaking at ~30 μm in dusty carbon-rich objects, and Goebel and Moseley (1985) proposed MgS as the carrier. MgS only shows the one resonance at ~30 μm, making it difficult to confirm that it is indeed the carrier. Not surprisingly, many challenges have been raised. Sloan et al. (2014) reviewed the arguments for and against MgS and concluded that it remains the best candidate.

MgS condenses at cool temperatures and would not be expected in optically thin dust shells, where the emission is dominated by warm grains close to the central star. The Magellanic samples show that MgS emission follows these expectations, with the ~30 μm feature more common and stronger in stars associated with more dust. When Goebel and Moseley (1985) proposed MgS as the carrier, they suggested that it might form in a surface reaction on already formed grains. The Magellanic samples show that as the strength of the MgS emission increases, SiC emission weakens, which is consistent with a layer of MgS forming on pre-existing grains (e.g. Lagadec et al., 2007; Leisenring et al., 2008; Zhukovska and Gail, 2008).

The MgS feature can grow to dominate the infrared emission from carbon-rich post-AGB objects, leading to concerns about whether enough S is available to explain the observed emission (e.g. Zhang et al., 2009). The abundance issue may be the strongest argument against MgS as the carrier of the ~30 μm feature. However, if the grains producing the feature only have MgS in a layer around a core of amorphous carbon and/or SiC, they will still produce an emission feature identical to that of a pure MgS grain, but without violating abundance constraints (Lombaert et al., 2012).

2.5. Calibrating dust-production rates

Using radiative transfer models, we can use infrared spectra and photometry of carbon stars to estimate how much dust they are producing. Applying that knowledge to the entire LMC or SMC leads to estimates of how dust input from evolved stars affects the dust balance in galaxies as a whole. Several papers show that while carbon stars dominate the measured dust input into the interstellar medium in both the LMC and SMC, they fall short of explaining the total observed interstellar dust mass in each galaxy (Matsuura et al., 2009, 2013; Boyer et al., 2012; Gordon et al., 2014).

A major problem with estimating the amount of dust produced by carbon stars is our uncertainty about the appropriate optical constants for amorphous carbon, which dominates the carbon-rich dust output. Work by Matsuura and collaborators relied on radiative transfer modeling by Groenewegen et al. (2007, 2009), which used the dust constants from Rouleau and Martin (1991). Boyer et al. (2012) used the grid of radiative transfer models developed by Srinivasan et al. (2011), which used constants from Zubko et al. (1996, their ACAR sample).

Groenewegen and Sloan (2017) have compared radiative transfer models using the two sets of constants. Fig. 4 shows that differences between the optical constants can lead to a difference of nearly an order of magnitude in total mass-loss rate! The Zubko constants require significantly less dust to explain the same emission, presumably because their laboratory samples were more graphitic and less amorphous. Generally, a grain with a more regular lattice structure should be a better conductor and thus a more efficient emitter and absorber. The extreme case of an ordered structure in carbon would be graphite, which consists of sheets of graphene with the carbon arranged in a hexagonal lattice. Martin and Rogers (1987) settled the debate over amorphous carbon versus graphite in circumstellar dust shells based on the lack of a narrow emission feature from graphite expected at 11.52 μm and the difficulties in fitting graphite to the dust continuum observed in dusty carbon stars. However, graphite is just an end state, and amorphous carbon really represents a spectrum of relative degrees of disorder. The bottom line is that we don't know how disordered the dust produced by a carbon star really is, and the greater the disorder, the more carbon is required to achieve the same emission and absorption. This uncertainty makes it difficult to quantify how carbon stars fit into the overall interstellar dust budget of galaxies.

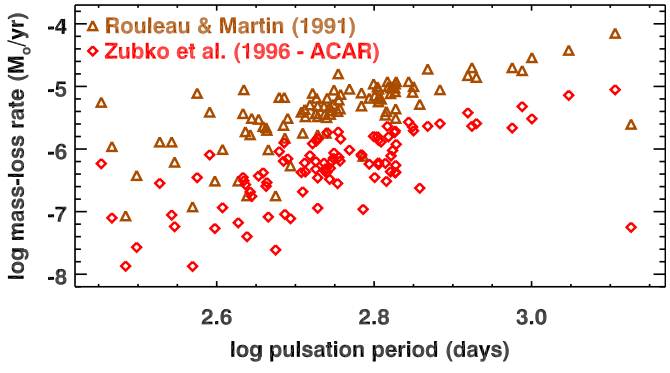

Fig. 4. A comparison of mass-loss rates determined from radiative transfer models using two sets of optical constants for amorphous carbon. The constants from Rouleau and Martin (1991) lead to estimates of the mass-loss rates up to nearly an order of magnitude higher than for the ACAR constants from Zubko et al. (1996).

3. Dust around carbon-rich post-AGB objects

When Gillett et al. (1973) discovered the unidentified infrared (UIR) emission features, they found them in the spectra of young, carbon-rich PNe. The family of UIR features includes emission at 3.3, 3.4, 6.2, 7.6–7.9, 8.6, 11.2, and 12.7 μm, to list just the stronger features, and the carrier has been identified as polycyclic aromatic hydrocarbons (PAHs; Leger and Puget, 1984; Allamandola et al., 1985). This identification has generated a great deal of controversy over the years, but PAHs best describe the properties that the carrier must have (Allamandola et al., 1989). Laboratory samples of PAHs reproduce the observed spectral features. The stability of aromatics (as opposed to aliphatics) in the harsh UV fields where the UIR features are observed strengthens the case. Consideration of the energetics requires that the carrier be at the threshold between large molecules and very small grains, which mean that the aromatic hydrocarbon molecules must consist of many aromatic rings, that is, they must be polycyclic. Various other hydrocarbon-based carriers have been proposed, but for them to generate the observed UIR features, they must be dominated by PAHs.

Thus PAHs appear to be the last surviving form of hydrocarbons as a carbon-rich AGB star evolves through the post-AGB phase into a young PN. Carbonaceous grains can take a variety of forms along this evolutionary path.

3.1. PAHs around post-AGB objects are not purely aromatic

Peeters et al. (2002) classified the spectra of PAHs from the Short-Wavelength Spectrometer (SWS) on the *Infrared Space Observatory* in three groups. In Class A PAH spectra, the 7.6–7.9 μm region shows a peak at ~7.65 μm, while in Class B spectra, the peak is shifted to ~7.85 μm. Other features shift as well, as Fig. 5 (left) shows. Generally, Class A PAHs are associated with pre-main-sequence objects like H II regions, while Class B PAHs are associated with post-main-sequence objects like PNe, but the SWS sample includes many exceptions. Only two of the SWS spectra were Class C, with the 7.6–7.9 μm complex shifted to ~8.2 μm. Both were carbon-rich post-AGB objects.

The spectroscopic sample from the IRS has helped us understand that the shift from Class B to Class C PAHs results from an increase in the amount of aliphatics in the hydrocarbon mix. Sloan et al. (2005) reported several Herbig AeBe stars that showed spectra intermediate between Class B and C and noted that the spectrum most like Class C was excited by the coolest radiation field in the sample. Sloan et al. (2007) added several Class C spectra to the sample, all of which had radiation fields much cooler than the usual PAH sources. They hypothesized that aliphatic bonds normally destroyed in hotter environments were surviving around the Class C sources and as a result, the PAH features were shifted to longer wavelengths. Laboratory data by Pino et al. (2008) confirmed that increasing the aliphatic fraction within a PAH sample did indeed shift emission features to longer wavelengths.

The key point is that a cooler radiation field allows more than just PAHs to survive. What else do we see from carbon-rich dust in post-AGB objects?

3.2. The 21 μm spectra and aliphatics

Galactic carbon-rich post-AGB objects sometimes show unusual spectra with an unidentified 21 μm feature, which was discovered by Kwok et al. (1989). Volk et al. (2011) found several spectra from Magellanic post-AGB objects that also have the 21 μm feature. Fig. 6 (left) shows an example. These spectra have several features in common.

First, the PAH emission is unusual. Matsuura et al. (2014) created a new Class D to describe the PAHs. Sloan et al. (2014) found that the class could be broken into two, as Fig. 5 (right) shows. Generally, Class D PAHs show excess emission which fills in the valley between the 7.6–7.9 μm PAH complex and the 8.6 μm PAH feature. They also differ at 11–13 μm. PAHs show strong emission at 11.2 μm with a dip to the much weaker feature at 11.9 μm, then a rise to 12.7 μm, but Class D PAHs show much more emission between 11.2 and 12.7 μm. Class D2 PAHs can be distinguished from Class D1 because the features normally seen at 11.9, and 12.7 μm have shifted to ~12.4 and 13.2 μm. The reason for this shift is not known.

Second, the 21 μm spectra can show several additional features not usually seen in more traditional PAH spectra. Strong emission features from aliphatic hydrocarbons can appear at 6.85 and 7.25 μm, but these are not always present. Most 21 μm spectra show features at 15.8 and 17.1 μm, and Sloan et al. (2014) found that aliphatic chains with triple C—C bonds reproduce these features. If an aliphatic chain ends with a triple C—C bond, the feature appears at 15.8 μm, and if the triple bond is shifted one in from the end, the feature shifts to ~17.1 μm.

Thus we have evidence linking the 21 μm feature to aliphatic hydrocarbons. Some aliphatic species might actually be the carrier of the 21 μm feature, or perhaps some other carrier is responsible that only appears when aliphatic hydrocarbons are present.

3.3. Fullerenes and related spectra

Young carbon-rich PNe can show fullerenes in their spectra. Cami et al. (2010) discovered fullerenes in the IRS spectrum of the Galactic PN Tc 1. Their identification was based on multiple features at 7.0, 8.5, 17.4, and 18.9 μm. Several PNe with fullerenes are now known in the Magellanic Clouds (García-Hernández et al., 2010, 2011; Sloan et al., 2014).

Sloan et al. (2014) investigated the photometric properties of Magellanic PNe with fullerenes and found that they tend to be bluer at optical wavelengths than otherwise similar PNe, suggesting that we may be observing fullerenes when we have a clear line of sight to the central regions of the nebula. The infrared colors of the fullerene sources are more tightly distributed than for similar non-fullerene sources, which again suggests that an unknown, but specific, geometry is required.

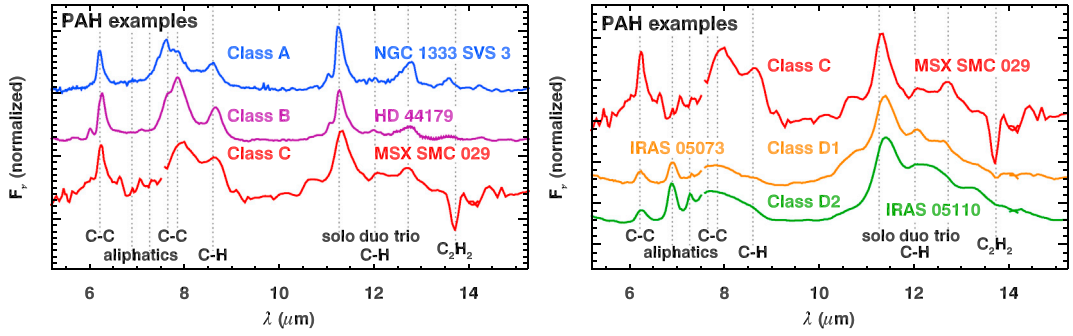

Fig. 5. Examples of PAH classes A, B, C (left), D1, and D2 (right), with the assignments for the identified modes. The 8.6 μm PAH feature is an in-plane C–H bending mode, while the wavelength of the out-of-plane C–H bending modes at 11–13 μm depends on the number of adjacent H atoms on a given aromatic ring. The 13.7 μm absorption band seen in post-AGB objects is from gaseous acetylene, and aliphatic hydrocarbon modes appear in some post-AGB spectra at 6.85 and 7.25 μm.

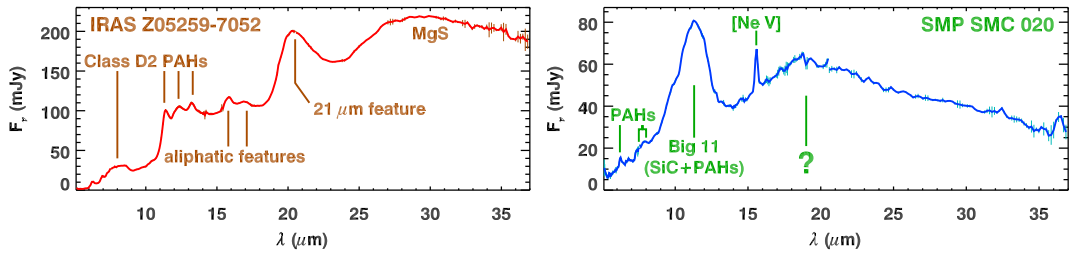

Fig. 6. Two examples of spectra from carbon-rich post-AGB objects, with a typical spectrum with a 21 μm feature on the left and a spectrum with one of the stronger Big-11 features and accompanying 18 μm shoulder on the right.

Galactic PNe with fullerenes provide another clue. Otsuka et al. (2014) found that they tend to lie outside the Solar circle, suggesting that fullerenes are more likely to be seen in metal-poor PNe.

Young carbon-rich PNe can show emission from fullerenes, and they can also have an unusually strong SiC feature which can be described as the "Big-11" feature. The strength of the Big-11 feature generally rises as the fullerene feature weakens. Bernard-Salas et al. (2009) pointed out the strength of this feature in Magellanic spectra compared to Galactic objects, even though abundance arguments would lead one to expect the opposite behavior. Sloan et al. (2014) showed that the Big-11 feature is a combination of SiC and PAH emission and suggested a solution to this problem similar to that for the MgS feature at ~30 μm. In young PNe, photoprocessing of grains composed of a mixture of SiC and amorphous carbon may preferentially remove the hydrocarbon component, leaving the grains with a coating dominated by SiC.

Most spectra with the Big-11 feature also have a shoulder at 18 μm, and Bernard-Salas et al. (2009) wondered if it might be due to silicates. Sloan et al. (2014) argued against this possibility since the PNe with the feature are carbon-rich. However, the case for PNe with dual chemistry continues to grow. PNe with dual chemistry are common in the Galactic Bulge (Gutenkunst et al., 2008; Perea-Calderón et al., 2009). The young carbon-rich Galactic PN BD+30 3639 is particularly interesting. Guzman-Ramirez et al. (2015) uncovered evidence that it is surrounded by a cold reservoir of silicate grains, and they argued that the silicates may be remnants of the dust produced while the central star was still on the AGB and before it became a carbon star. It remains to be investigated whether or not silicate grains in Magellanic PNe could be cold enough to emit at 18 μm but not show significant emission at 10 μm. Fig. 6 (right) presents the spectrum of a PN in the SMC with an unusually strong Big-11 feature and the clearest example of the 18 μm shoulder. Could this object be a dual-chemistry source due to dust surviving from its oxygen-rich phase on the AGB?

4. Conclusion

Infrared spectroscopy of evolved carbon-rich objects reveals a wealth of compositions, and while recent progress has disentangled several problems, many more remain. The discovery of fullerenes has certainly been exciting, but we still do not understand why we see fullerenes in some objects and not others. We clearly see an increase in the ratio of aliphatic to aromatic hydrocarbons as the radiation field grows cooler and the amount of photoprocessing drops. The association of some of these aliphatic features with the 21 μm feature helps constrain its carrier, but we still have not identified it. For carbon stars on the AGB, amorphous carbon dominates the dust, but until we understand its structure, we remain uncertain how much dust these stars can contribute back to their environment as they die. In both the post-AGB and AGB objects, the most important question is "How ordered is the structure of the carbon?" On one end of the spectrum, we have PAHs and graphite, and on the other, aliphatic hydrocarbons or completely amorphous carbon.

The answers to the questions raised in this review will require new observations in some cases and further laboratory work in others. The upcoming launch of the James Webb Space Telescope promises great progress observationally. As one example, the medium-resolution spectroscopic mode on Mid-Infrared Instrument (MIRI) will produce spectral/imaging data cubes from 5 to 28 μm of a field up to ~7 × 8" in size. With this mode, the various spectral emission features observed in carbon-rich post-AGB objects (PAHs, 21 μm feature, fullerenes, etc.) can be mapped, providing further constraints on their carriers and how they form. One of the questions in need of attention in the laboratory is the relative sturdiness of aliphatic and aromatic hydrocarbons in harsh radiative environments. Another is to better quantify how the overall opacity of amorphous carbon depends on the ratio of aliphatic to aromatic bonds. And finally, how can we distinguish the composition of amorphous carbon spectroscopically?

References

Alcock, C., Axelrod, T.S., Bennett, D.P., et al., 1992. ASPC 34, 193.
Allamandola, L.J., Tielens, A.G.G.M., Barker, J.R., 1985. ApJ 290, L25.
Allamandola, L.J., Tielens, A.G.G.M., Barker, J.R., 1989. ApJS 71, 733.
Bernard-Salas, J., Peeters, E., Sloan, G., et al., 2009. ApJ 699, 1541.
Blanco, B.M., Blanco, V.M., McCarthy, M.F., 1978. Nature 271, 638.
Blanco, V.M., Blanco, B.M., McCarthy, M.F., 1980. ApJ 242, 938.
Boyer, M.L., Srinivasan, S., Riebel, D., et al., 2012. ApJ 748, 40.
Cami, J., Bernard-Salas, J., Peeters, E., Malek, S.E., 2010. Science 329, 1180.
Cioni, M.-R.L., Habing, H.J., 2003. A&A 402, 133.
Forrest, W.J., Houck, J.R., McCarthy, J.F., 1981. ApJ 248, 195.
Fraser, O.J., Hawley, S.L., Cook, K.H., Keller, S.C., 2005. AJ 129, 768.
García-Hernández, D.A., Manchado, A., García-Lario, P., et al., 2010. ApJ 724, L39.
García-Hernández, D.A., Iglesias-Groth, S., Acosta-Pulido, J.A., et al., 2011. ApJ 737, L30.
Gillett, F.C., Forrest, W.J., Merrill, K.M., 1973. ApJ 183, 87.
Goebel, J.H., Moseley, S.H., 1985. ApJ 290, L35.
Gordon, K.D., Roman-Duval, J., Bot, C., et al., 2014. ApJ 797, 85.
Groenewegen, M.A.T., Sloan, G.C., Soszyński, I., Petersen, E.A., 2009. A&A 506, 1277.
Groenewegen, M.A.T., Wood, P.R., Sloan, G.C., et al., 2007. MNRAS 376, 313.
Groenewegen, M.A.T., Sloan, G.C., 2017. A&A (submitted).
Gruendl, R.A., Chu, Y.-H., Seale, J.P., et al., 2008. ApJL 688, L9.
Gutenkunst, S., Bernard-Salas, J., Pottasch, S.R., Sloan, G.C., Houck, J.R., 2008. ApJ 680, 1206.
Guzman-Ramirez, L., Lagadec, E., Wesson, R., et al., 2015. MNRAS 451, L1.
Habing, H., 1996. Astron. Astroph. Rev. 7, 97.
Houck, J.R., Roellig, T.L., van Cleve, J., et al., 2004. ApJS 154, 18.
Karakas, A., Lattanzio, J.C., 2007. PASA 24, 103.
Kwok, S., Hrivnak, B.J., Volk, K.M., 1989. ApJ 345, L51.
Lagadec, E., Zijlstra, A.A., Sloan, G.C., et al., 2007. MNRAS 376, 1270.
Leger, A., Puget, J.L., 1984. A&A 137, L5.
Leisenring, J.M., Kemper, F., Sloan, G.C., 2008. ApJ 681, 1557.
Lombaert, R., de Vries, B.L., de Koter, A., et al., 2012. A&A 544, L18.
Martin, P.G., Rogers, C., 1987. ApJ 322, 374.
Matsuura, M., Barlow, M.J., Zijlstra, A.A., et al., 2009. MNRAS 396, 918.
Matsuura, M., Bernard-Salas, J., Lloyd Evans, T., et al., 2014. MNRAS 439, 1472.
Matsuura, M., Woods, P.M., Owen, P., 2013. MNRAS 429, 2527.
Meixner, M., Gordon, K.D., Indebetouw, R., et al., 2006. AJ 132, 2268.
Otsuka, M., Kemper, F., Cami, J., Peeters, E., Bernard-Salas, J., 2014. MNRAS 437, 2577.
Peeters, E., Hony, S., Van Kerckhoven, C., et al., 2002. A&A 390, 1089.
Perea-Calderón, J.V., García-Hernández, D.A., García-Lario, P., Szczerba, R., Bobrowsky, M., 2009. A&A L5.
Pino, T., Dartois, E., Cao, A.-T., et al., 2008. A&A 490, 665.
Rouleau, F., Martin, P.G., 1991. ApJ 377, 526.
Sloan, G.C., Jura, M., Duley, W.W., et al., 2007. ApJ 664, 1144.
Sloan, G.C., Keller, L.D., Forrest, W.J., et al., 2005. ApJ 632, 956.
Sloan, G.C., Kraemer, K.E., Matsuura, M., et al., 2006. ApJ 645, 1118.
Sloan, G.C., Kraemer, K.E., McDonald, I., et al., 2016. ApJ 826, 44.
Sloan, G.C., Kraemer, K.E., Wood, P.R., et al., 2008. ApJ 686, 1056.
Sloan, G.C., Lagadec, E., Kraemer, K.E., et al., 2015. Why galaxies care about AGB stars III. In: Kerschbaum, F., Hron, J., Wing, R. (Eds.), ASP Conf. Series, vol. 497, p. 429.
Sloan, G.C., Lagadec, E., Zijlstra, A.A., et al., 2014. ApJ 791, 28.

Sloan, G.C., Matsuura, M., Lagadec, E., et al., 2012. ApJ 752, 140.
Soszyński, Udalski, A., Szymański, M.K., et al., 2009. AcA 59, 335.
Srinivasan, S., Sargent, B.A., Meixner, M., 2011. A&A 532, 54.
Udalski, A., Szymanski, M., Kaluzny, J., Kubiak, M., Mateo, M., 1992. AcA 42, 253.
Volk, K., Hrivnak, B.J., Matsuura, M., et al., 2011. ApJ 735, 127.
Werner, M.W., Roellig, T.L., Low, F.J., et al., 2004. ApJS 154, 1.
Zhang, K., Jiang, B.W., Li, A., 2009. ApJ 702, 680.
Zhukovska, S., Gail, H.-P., 2008. A&A 486, 229.
Zijlstra, A.A., Matsuura, M., Wood, P.R., et al., 2006. MNRAS 370, 1961.
Zubko, V.G., Mennella, V., Colangeli, L., Bussoletti, E., 1996. MNRAS 282, 1321.